JACS
JOURNAL OF THE AMERICAN CHEMICAL SOCIETY
Article
pubs.acs.org/JACS

Liquid Cell Transmission Electron Microscopy Study of Platinum Iron Nanocrystal Growth and Shape Evolution

Hong-Gang Liao and Haimei Zheng*

Materials Sciences Division, Lawrence Berkeley National Laboratory, Berkeley, California 94720, United States

Supporting Information

ABSTRACT: We study solution growth of platinum iron nanocrystals in situ in a liquid cell by using transmission electron microscopy. By varying the oleylamine concentration, we observed that platinum iron nanoparticle growth follows different trajectories with diverse shape evolution. With 20% oleylamine, three stages of growth were observed: (i) nucleation and growth of platinum iron nanoparticles in the precursor solution; (ii) nanowire formation by shape-directed nanoparticle attachment; and (iii) breakdown or shrinkage of the nanowires into individual nanoparticles with large size distribution. With 30% oleylamine, formation of platinum iron nanowires similar to that with 20% oleylamine was observed. However, those nanowires do not break down or shrink, which suggests that nanowires are stabilized by oleylamine as surfactant binding on the surface. With 50% oleylamine, after the individual nanoparticles are formed, they do not merge into nanowires. The shape of the nanoparticle is strongly influenced by the neighboring nanoparticles due to stereo-hindrance effects. Real-time observation of the dynamic growth process sheds light on the controllable synthesis of nanomaterials.

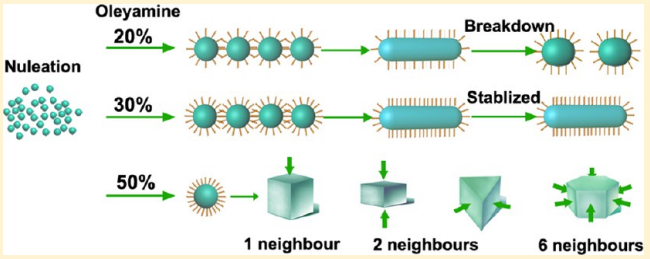

INTRODUCTION

The ability to control the size and shape of nanocrystals provides flexibility in engineering their electronic, catalytic, and optical properties. The synthesis of nanocrystals with tunable size and shape has been an active foreland field of research, which has attracted great attention for both fundamental study and applications. Over the past two decades, colloidal synthesis has achieved remarkable success in delivering a wide range of metal, semiconductor, and dielectric nanoparticles with monodisperse size and various fascinating shapes.[1−7] However, the mechanisms of nanocrystal growth are not yet well understood. Nanocrystal growth is a complex process involving the arrangement of a large number of molecules near the crystal surface, and it is further complicated by the interaction of the nanocrystal with its environment. Factors such as precursor concentration, temperature, surfactants, etc.[8−11] can affect the chemical potential of crystallization in liquids; thus, the size and shape of the nanocrystals formed differ under different growth conditions. An understanding of the mechanism of colloidal nanocrystal morphology evolution is essential for achieving nanocrystals with the designed architectures to meet the needs for advanced applications.

It has been reported in many previous studies that surfactants play an important role during nanocrystal growth.[10,12−15] This is likely because the absorption of surfactant molecules modifies the surface properties of the nanocrystals. Changes in the electronic structure, energy level, and reactivity of surface atoms due to surface absorption drastically affect nanocrystal growth. Future design of novel synthesis routes requires a detailed understanding of how the size and shape of nanocrystals evolve under the influence of surfactant molecules. However, this has been challenging due to the lack of capability to monitor the dynamic processes of nanocrystal growth in solution.

Recent developments in transition electron microscopy (TEM) allow the study of single-particle growth trajectories in situ,[16−19] which provides the opportunity to address the above issue. A microfabricated environmental cell operated inside a transission electron microscopy can encapsulate a small amount of liquids, where the growth of nanocrystals is initiated either by thermo reduction[20] or an electron beam.[17] The dynamic growth process can be studied in real time with sub-nanometer resolution. Although the growth conditions in a liquid cell can be different from those for synthesis in a flask, many recent studies show that nanocrystals synthesized in a liquid cell resemble those from flask synthesis.[21,22] In situ study of nanocrystal growth in a liquid cell enlightens us on the fundamental rules governing colloidal nanocrystal growth.

In this work, we study the growth of platinum iron nanocrystals by using liquid cell TEM. By systematically varying the oleylamine concentration while maintaining the same precursor concentration, temperature, and electron beam conditions, we track the growth trajectories of nanoparticles and monitor their shape evolution. Our direct observation reveals details on how oleylamine affects nanocrystal shape evolution and how the shape of a nanocrystal is further influenced by neighboring nanoparticles within a close distance. Oleylamine is widely used as a surfactant in colloidal synthesis

Received: October 28, 2012
Published: March 11, 2013

   dx.doi.org/10.1021/ja310612p | J. Am. Chem. Soc. 2013, 135, 5038−5043

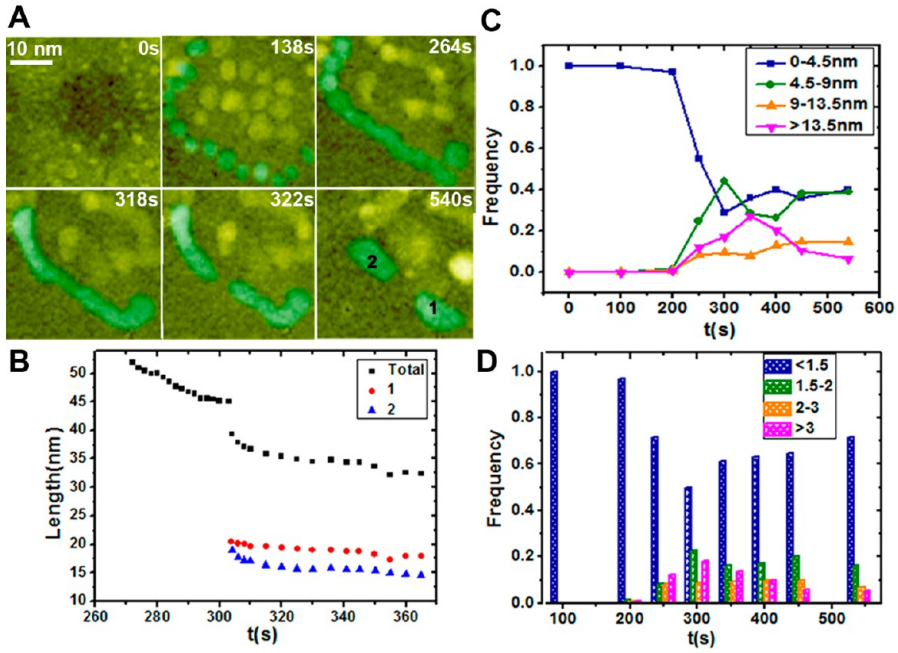

Figure 1. Growth of platinum iron nanoparticles in a solvent with 20% oleylamine. (A) Sequential images show the evolution of platinum iron nanocrystals from the formation of individual nanoparticles to a nanowire by nanoparticle attachment, followed by breakdown and shrinkage of the nanowire into nanoparticles. Nanoparticles are highlighted in green. (B) Changes in the length of the nanowire in (A) as a function of time. (C) Statistics of the length of the nanoparticles as a function of time. (D) Statistics of the aspect ratio of the nanoparticles as a function of time (468 individual nanoparticles were measured at the early stage).

of platinum iron nanoparticles. This study provides valuable information on the effects of surfactant on nanoparticle growth through in situ observation.

■ MATERIALS AND METHODS

All chemicals, including Pt(acetylacetonate)$_2$ (99%, Aldrich), Fe-(acetylacetonate)$_2$ (99%, Aldrich), pentadecane (99%, Aldrich), and oleylamine (70%, Aldrich), are used as received.

The growth solution is prepared by dissolving Pt(acetylacetonate)$_2$ (20 mg/mL) and Fe(acetylacetonate)$_2$ (20 mg/mL) in organic solvent. Solvent mixtures of oleylamine and pentadecane with the oleylamine concentration of 20%, 30%, and 50% (in other words, the volume ratio of oleylamine:pentadecane is 2:8, 3:7, and 5:5) are used to investigate surfactant effects. About 50 nL of growth solution is loaded into one of the reservoirs in a liquid cell. The solution is drawn into the cell by capillary force and forms a liquid layer (120 nm) sandwiched between two silicon nitride membranes (each with a thickness of 13 nm) at the window. We fill the other reservoir with the same growth solution before the liquid cell is sealed using epoxy. The liquid cell is then loaded into the microscope as a standard TEM sample for imaging. A JEOL 3010 transmission electron microscopy operated at 300 kV and a beam current density of $(1-8) \times 10^5 A/m^2$ is maintained for the study. However, the intensity can vary briefly at the initial exposure to the electron beam during the time period required to focus for imaging (a few seconds). A Philips CM200 transmission electron microscope with an energy dispersive X-ray spectroscopy (EDS) detector is used for elemental analysis following the in situ experiments.

Liquid Cell Fabrication and Growth Solution Loading for TEM. Liquid cells are fabricated by following a process similar to one described in a previous publication.[17] We use ultrathin silicon wafers (100 μm, 4-in., p-doped) purchased from Virginia Semiconductor (Fredericksburg, VA) and deposit low-stress silicon nitride membranes with a thickness of 13 nm on the silicon wafers. Here, the use of ultrathin silicon nitride membranes effectively improves the spatial resolution of the liquid cell. The subsequent fabrication processes include lithographic patterning, wet KOH etching of silicon, and liquid cell bonding using an indium thin-film spacer. The indium is deposited by sputtering, and it acts as a spacer as well as the sealing material for the liquid cell. A 120 nm spacing is used for the current experiments, although different thicknesses can be achieved. All the fabrication processes are conducted at the Nanofabrication Lab of the University of California at Berkeley. The liquid loading is facilitated by using a syringe and Teflon nanotube (purchased from Cole-Parmer, Vernon Hills, IL) to control the size of liquid droplets.

Initiation of the Growth of Platinum Iron Nanocrystals. The growth of platinum iron nanocrystals in a liquid cell is initiated by electron beam illumination of the growth solution. The reduction of Pt(acetylacetonate)$_2$ and Fe(acetylacetonate)$_2$ precursor (Pt^{2+},Fe^{2+}) to metal (Pt^0,Fe^0) can be from either (i) oleylamine-assisted metal ion reduction at elevated temperature or (ii) direct reduction by electron beam.[17] Since the liquid temperature is low,[17] we believe the reduction of Pt^{2+} and Fe^{2+} by electron beam, i.e., from primary electrons or the solvated electrons from elastic scattering,[23] is predominant. It is noted that growth by monomer attachment becomes negligible during the later stage of growth by nanoparticle attachment. Although the electron beam plays an important role during nanoparticle growth, the different shape evolution of platinum iron nanocrystals in this work is clearly governed by the variations in oleylamine concentration.

TEM Imaging and Image Processing. All movies were recorded using a Gatan SC200 camera (fiber optical charge-coupled device (CCD)), which allows recording at 30 frames per second. Movies S1–S5 (Supporting Information) were recorded under a 3010 JEOL transmission electron microscope, which shows sub-nanometer spatial resolution. All movies play 30 times faster than the real speed and are compressed to larger pixel sizes to reduce the file size. Image contrast of all movies is as-recorded. Nanocrystals in the sequential images in Figures 1, 2, 4, and 5 are highlighted in green by a false coloring process using Photoshop software. All original images can be retrieved; see movies S1–S5.

■ RESULTS AND DISCUSSION

We study the growth of platinum iron nanoparticles in a liquid cell by varying the concentration of oleylamine. First, 20% of oleylamine is used, and the growth trajectory of a platinum iron

dx.doi.org/10.1021/ja310612p | J. Am. Chem. Soc. 2013, 135, 5038–5043

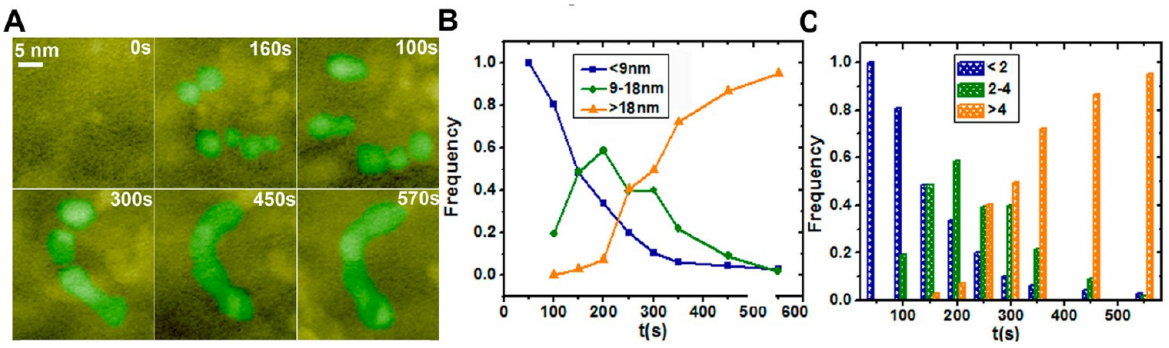

Figure 2. Growth of platinum iron nanoparticles in a solvent with 30% oleylamine. (A) Sequential images showing the growth of platinum iron nanowires. Nanoparticles are highlighted in green. (B) Statistics of the length of nanowires as a function of time. (C) Statistics of the aspect ratio of nanowires as a function of time (165 individual nanoparticles were measured at the early stage).

nanoparticle is depicted in Figure 1A (also see movie S1 for details). Three distinct stages of growth can be identified. During the first stage (typically 0–250 s), many small nanoparticles are formed when the Pt and Fe precursors are reduced by electron beam illumination. Some of them grow by monomer attachment; others undergo coalescence. The nanoparticles merged by coalescence relax into spherical nanoparticles, and the relaxation time increases as particle size increases. The growth during this stage is similar to what was observed in previous studies.[17,24] When these nanoparticles reach the size of 4 ± 0.4 nm, the second stage of growth (250–315 s) begins. Nanoparticles interact with each other and form nanoparticle chains. Unlike in the first stage of growth, dimers do not quickly relax into a sphere. Instead, a trimer is formed when an additional nanoparticle connects to the dimer end, and the additional end-to-end attachments generate a nanoparticle chain. A long nanoparticle chain can also form when short chains of nanoparticles connect to each other. Subsequently, adjacent nanoparticles within the chain connect with each other, forming a neck at which, presumably, surfactant molecules are excluded. Further mass redistribution eliminates the neck, and a smooth nanowire is formed. However, these nanowires grown in 20% oleylamine are not stable in the solution. Striking shape evolution of the nanowires is observed in the following stage.

During the third stage of growth (315–540 s), the short nanowires shrink into nanoparticles with a diameter of about 10–15 nm. A long nanowire can break down into two or more pieces. As shown in Figure 1A, a neck is formed in the middle of the wire while the nanowire is shrinking. As the neck develops, the wire breaks into two pieces. The change of one wire's length as a function of growth time (Figure 1B) clearly shows that there is a sudden decrease of wire length corresponding to the breakdown of the nanowire. Each piece continues to shrink until two nanoparticles are formed.

The change of nanowire length as a function of time is plotted in Figure 1C. It is clear that at the early stage the system is dominated by single nanoparticles. As the growth proceeds, a significant population of short chains (4.5–9 nm) and long chains (>13.5 nm) of nanoparticles appears. When most nanowires relax or break down into pieces, a large size distribution of nanoparticles is observed. Figure 1D shows the aspect ratio of the nanowires as a function of time, where a single nanoparticle is represented by an aspect ratio of less than 1.5 and those with an aspect ratio larger than 3 are considered as nanowires. The population of single nanoparticles decreases during the nanowire formation (stages I and II), and it increases as nanowires break down (stage III). An opposite trend of the evolution of nanowires is observed.

As the concentration of oleylamine increases to 30%, platinum iron nanowires are formed. Figure 2A shows the growth trajectories of a platinum iron nanowire (also see movie S2 for details). The statistical changes of nanowire length and aspect ratio as a function of growth time are plotted in Figure 2B,C. It is clear that only individual nanoparticles are observed during the early stage of growth. As growth proceeds, dimers and trimers are dominant in the solution. At the end, only long nanowires with aspect ratio larger than 4 are observed, and they are stable for an extended period of time. The evolution from single nanoparticles to long-chain nanowires is the same as the first two stages of growth with 20% oleylamine. However, nanowires grown in solutions with 30% oleylamine are stable, without shrinkage or breakdown. Nanowire formation by shape-directed attachment of nanoparticle building blocks was described in a previous publication.[24]

We compare the stability of the nanowires grown with 20% oleylamine and those with 30% oleylamine. As shown in Figure 3, the breakdown of nanowires in the solution with 20% oleylamine is correlated with the length of the nanowire. A critical length of 35–40 nm is identified. Nanowires with length shorter than the critical length do not break down (they

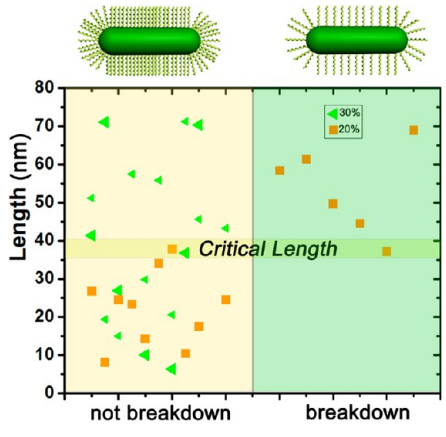

Figure 3. Stability of the nanowires synthesized in the solvent with 20% or 30% oleylamine. The orange squares show the nanowires formed with 20% oleylamine, and the green triangles show the nanowire formed with 30% oleylamine. Nanowires break down in the solution with 20% oleylamine, and a critical length of 35–40 nm is identified.

dx.doi.org/10.1021/ja310612p | J. Am. Chem. Soc. 2013, 135, 5038–5043

shrink), and nanowires longer than the critical length break down into pieces accompanied by shrinkage. Nanowires formed in a solution with 30% oleylamine do not break down or shrink, regardless of the length of the wire.

The structural deformation of the nanowire can be interpreted by Rayleigh–Plateau instability.[25,26] For a thin nanowire, since almost all atoms are near the surface, they can rearrange easily.[24] Thus, the structure of a nanowire during growth is highly flexible, similar to fluids. A cylindrical structure becomes unstable when the force due to surface tension exceeds the limit that leads to plastic flow. Consider a cylindrical wire of radius r and length L: the maximum stress that the wire can sustain before the onset of plastic flow is σ_Y (the yield strength). On the other hand, the surface-induced stress in a thin wire is σ_S/r, where σ_S is the surface tension. If $\sigma_S/r > \sigma_Y$, it is expected that the wire undergoes plastic flow, which can lead to instability of the object in the absence of other stabilizing mechanisms. If $L > 2\pi r$, the cylinder tends to break down with respect to perturbations, as in the Rayleigh instability of a column of fluid. This has been used to explain the metastability of metal nanowires.[27−31]

According the above Rayleigh–Plateau instability theory, the critical length (L_0) for nanowires to break down can be estimated by $L_0 = 2\pi r$. For nanowires grown in solution with 20% oleylamine, L_0 is estimated to be ∼14–17 nm ($r \approx 2.3$–2.8 nm). This is smaller than the experimental value, which is probably due to surfactant coverage on the nanowire surface modifying the surface tension. Nanowires longer than the critical length turn to break down, and when nanowires are shorter than the critical length they shrink. For the nanowires formed in the solution with 30% oleylamine, they do not break down or shrink into a sphere even with the same geometry. This implies that the higher surfactant coverage changes the surface tension so drastically that nanowires get stabilized.

When the concentration of oleylamine increases to 50%, only single nanoparticles are formed. Figure 4A shows sequential images of platinum iron nanoparticles during growth (also see movie S3 for details). Nanoparticles can align to form a chain, but they do not merge to form a wire. This is probably due to the high concentration of surfactant stabilizing the individual nanoparticles in the solution. When more nanoparticles are assembled, a two-dimensional (2D) film of nanoparticles is observed. During the assembly of nanoparticles, motion of the nanoparticles is restricted to near the substrate surface, likely due to the strong interaction between nanoparticles and the substrate. The particle size distributions with time are plotted in Figure 4B, which shows the size focusing during growth. The shape of the nanoparticles evolves from spherical to hexagonal. The shape of a nanocrystal within the 2D film is highly influenced by the neighboring nanoparticles due to the "stereo-hindrance effect".[32,33]

EDS studies of nanocrystal ensembles (Figure S1) confirm that nanocrystals are composed of Pt and Fe with an atomic ratio of roughly 3:1 (75 ± 5% of Pt). Composition inhomogeneity has been observed in individual nanoparticles during the early stage of growth. However, mass redistribution can eventually result in a more homogeneous nanoparticle (Figure S2).

The stereo-hindrance effect is more obvious when nanoparticles are assembled into different geometries. Figure 5A,B shows the shape evolution of a nanoparticle within a chain and another nanoparticle at the end of the chain. The particle in the middle of the chain evolves into a rectangular shape, and the

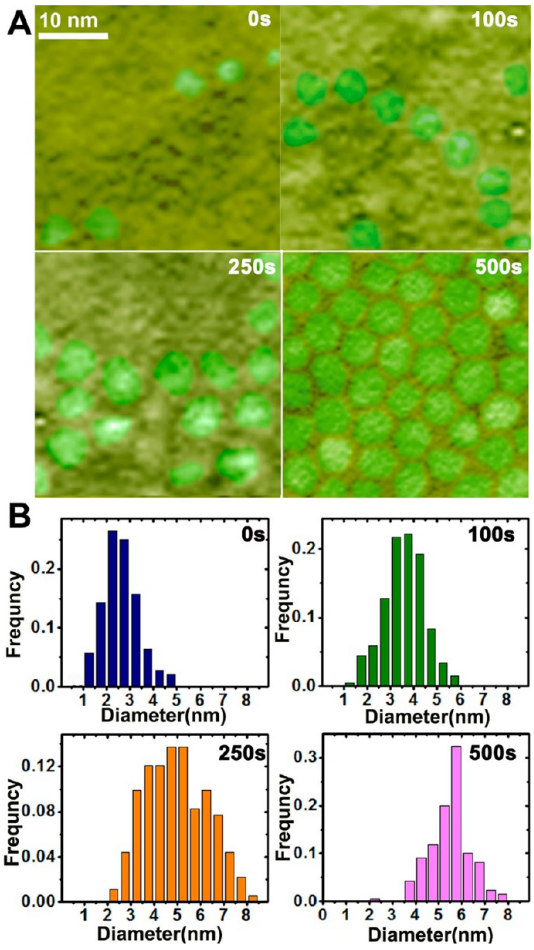

Figure 4. Growth of platinum iron nanoparticles in a solvent with 50% oleylamine. (A) Sequential images showing the growth of platinum iron nanocrystals. Nanoparticles are highlighted in green. (B) Nanoparticle size distribution during the growth (203 individual nanoparticles were measured at the early stage).

one at the end of the chain develops into a square shape. Figure 5C,D show the diameters of the two nanoparticles changing along the length and width directions. The growth rates along both directions of the nanoparticle at the end are almost identical. For the nanoparticle in the middle, growth along the width of the particle ceases when it reaches 1–2 nm close to the neighbors, while growth along the other direction continues. The results suggest that a high concentration of oleylamine can prevent nanoparticles from attaching to neighboring nanoparticles. However, the effect of oleylamine on the shape evolution of a nanoparticle is secondary to the effect of the neighboring nanoparticles. We further found that, when nanoparticles nucleate and grow on the substrate, forming a circle, each nanoparticle develops into a trapezoid shape, as shown in Figure 5E. The changes in length and width of a nanoparticle along the growth trajectory are plotted in Figure 5F, which shows that there is a continuous increase along the length, while growth along the width is restricted due to the neighboring effects.

Figure 6 summarizes the effects of neighboring nanoparticles on the shape evolution of a nanoparticle. The stereo-hindrance effect takes place when there is more than one neighboring nanoparticle. The shape of a nanoparticle is defined by the relative position of neighboring nanoparticles. When the

dx.doi.org/10.1021/ja310612p | J. Am. Chem. Soc. 2013, 135, 5038–5043

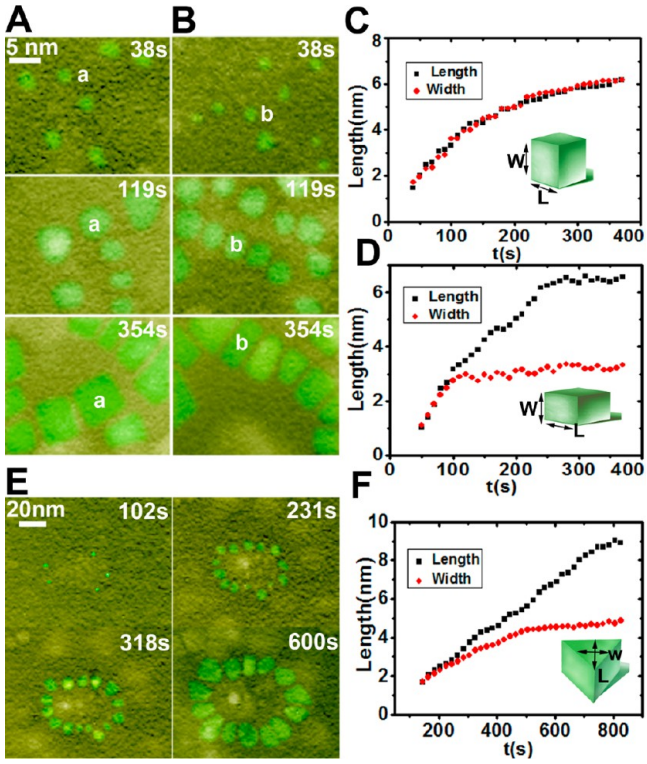

Figure 5. Growth of platinum iron nanoparticles in solutions with 50% oleylamine. (A,B) Sequential images showing the growth of platinum iron nanocrystals. Two nanoparticles, (a) at the end and (b) in the middle of the chain, are highlighted. (C,D) Changes of length and width of the two nanoparticles in (A) and (B) as a function of time. (E) Sequential images showing the formation of platinum iron nanoparticles in a circle. (F) Changes in the length and width of the nanoparticle highlighted in (E) as a function of time.

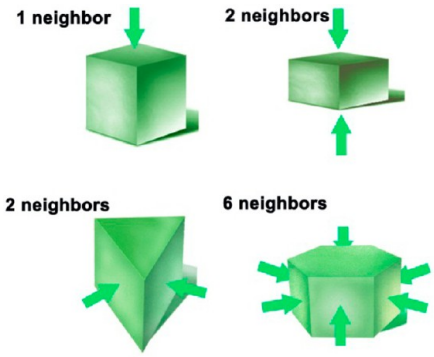

Figure 6. Schematics showing the stereo-hindrance effects during growth.

nanoparticle and two neighbors are in a straight line, the nanoparticle develops into a rectangle shape. When the nanoparticle and two neighbors form a curve, the particle develops into a wedge shape. A hexagonal nanoparticle is achieved when there are six neighboring nanoparticles. It is noted that the stereo-hindrance effect happens only when the relative position of the nanoparticles does not change for a period of time. As shown in movie S3, although some nanoparticles are aligned into a chain, the shape of the nanoparticles evolves differently from those in a chain, since the chain rapidly falls apart (the relative position of the nanoparticles changes). This implies that stereo-hindrance effects can be reduced if vigorous stirring of the growth solution is employed during synthesis. The benefits of stirring the growth solution during nanocrystal synthesis, however, often refer to achieving a more homogeneous concentration of nanoparticles without aggregation. For example, it has been discussed in previous studies that the stir speed affects the size and shape of the nanocrystals.[34−36]

CONCLUSIONS

With real-time observation of the growth trajectories of platinum iron nanoparticles using liquid environmental cell TEM, we have studied the shape evolution of nanocrystals with various oleylamine concentrations. Oleylamine can help to stabilize nanoparticles in a solvent. With a relatively low concentration of oleylamine (20%), after nanoparticles are attached end-to-end to form a nanowire, the nanowire can subsequently shrink into particles or breakdown into pieces. Large size distributions of the nanoparticles are observed. When the concentration of oleylamine increases to 30%, nanoparticles can still merge into a nanowire, but the nanowire is stable, with no breakdown or shrinkage. As the concentration of oleylamine increases to 50%, the individual nanoparticles are stable in solution, and merging between nanoparticles at the later stage can be avoided. In summary, oleylamine plays an important role in controlling the size and shape of the nanocrystals. However, we also found that the oleylamine (surfactant) effect on the shape evolution of a nanoparticle is secondary to the effect from the neighboring nanoparticles. We have directly observed for the first time that neighboring particles can strongly influence the nanocrystal shape evolution due to the stereo-hindrance effects. In situ observation of the dynamic growth process deepens our understanding of nanocrystal growth mechanisms and points the way for synthesis of nanomateials with desired properties.

ASSOCIATED CONTENT

Supporting Information

EDS spectrum, HAADF images, and movies S1−S5. This material is available free of charge via the Internet at http://pubs.acs.org.

AUTHOR INFORMATION

Corresponding Author

hmzheng@lbl.gov

Notes

The authors declare no competing financial interest.

ACKNOWLEDGMENTS

We acknowledge the facility support of National Center for Electron Microscopy, Lawrence Berkeley National Laboratory (LBNL), which is funded by the U.S. Department of Energy under Contract No. DE-AC02-05CH11231. We thank the DOE Office of Science Early Career Research Program for funding support.

REFERENCES

(1) Ahmadi, T. S.; Wang, Z. L.; Green, T. C.; Henglein, A.; ElSayed, M. A. *Science* **1996**, *272*, 1924.
(2) Murray, C. B.; Kagan, C. R.; Bawendi, M. G. *Annu. Rev. Mater. Sci.* **2000**, *30*, 545.
(3) Puntes, V. F.; Krishnan, K. M.; Alivisatos, A. P. *Science* **2001**, *291*, 2115.
(4) Wang, Y.; Herron, N. *J. Phys. Chem.* **1991**, *95*, 525.

(5) Vossmeyer, T.; Katsikas, L.; Giersig, M.; Popovic, I. G.; Diesner, K.; Chemseddine, A.; Eychmuller, A.; Weller, H. *J. Phys. Chem.* **1994**, *98*, 7665.
(6) Stankovich, S.; Dikin, D. A.; Piner, R. D.; Kohlhaas, K. A.; Kleinhammes, A.; Jia, Y.; Wu, Y.; Nguyen, S. T.; Ruoff, R. S. *Carbon* **2007**, *45*, 1558.
(7) Weller, H. *Angew. Chem., Int. Ed. Engl.* **1993**, *32*, 41.
(8) Peng, X. G.; Manna, L.; Yang, W. D.; Wickham, J.; Scher, E.; Kadavanich, A.; Alivisatos, A. P. *Nature* **2000**, *404*, 59.
(9) Leff, D. V.; Brandt, L.; Heath, J. R. *Langmuir* **1996**, *12*, 4723.
(10) Nikoobakht, B.; El-Sayed, M. A. *Chem. Mater.* **2003**, *15*, 1957.
(11) Xiang, G. L.; Zhuang, J.; Wang, X. *Inorg. Chem.* **2009**, *48*, 10222.
(12) Becker, J.; Schubert, O.; Sonnichsen, C. *Nano Lett.* **2007**, *7*, 1664.
(13) Busbee, B. D.; Obare, S. O.; Murphy, C. J. *Adv. Mater.* **2003**, *15*, 414.
(14) Murphy, C. J.; San, T. K.; Gole, A. M.; Orendorff, C. J.; Gao, J. X.; Gou, L.; Hunyadi, S. E.; Li, T. *J. Phys. Chem. B* **2005**, *109*, 13857.
(15) Nikoobakht, B.; El-Sayed, M. A. *Langmuir* **2001**, *17*, 6368.
(16) Williamson, M.; Tromp, R.; Vereecken, P.; Hull, R.; Ross, F. *Nat. Mater.* **2003**, *2*, 532.
(17) Zheng, H. M.; Smith, R. K.; Jun, Y. W.; Kisielowski, C.; Dahmen, U.; Alivisatos, A. P. *Science* **2009**, *324*, 1309.
(18) Evans, J. E.; Jungjohann, K. L.; Browning, N. D.; Arslan, I. *Nano Lett.* **2011**, *11*, 2809.
(19) De Jonge, N.; Ross, F. M. *Nat. Nanotechnol.* **2011**, *6*, 695.
(20) Xin, H. L.; Zheng, H. *Nano Lett.* **2012**, *12*, 1470. Yuk, J. M.; Park, J.; Ercius, P.; Kim, K.; Hellebusch, D. J.; Crommie, M. F.; Lee, J. Y.; Zettl, A.; Alivisatos, A. P. *Science* **2012**, *336*, 61.
(21) Yuk, J. M.; Park, J.; Ercius, P.; Kim, K.; Hellebusch, D. J.; Crommie, M. F.; Lee, J. Y.; Zettl, A.; Alivisatos, A. P. *Science* **2012**, *336*, 61.
(22) Browning, N. D.; Bonds, M. A.; Campbell, G. H.; Evans, J. E.; LaGrange, T.; Jungjohann, K. L.; Masiel, D. J.; McKeown, J.; Mehraeen, S.; Reed, B. W.; Santala, M. *Curr. Opin. Solid State Mater. Sci.* **2012**, *16*, 23.
(23) Egerton, R. F.; Li, P.; Malac, M. *Micron* **2004**, *35*, 399.
(24) Liao, H.-G.; Cui, L.; Whitelam, S.; Zheng, H. *Science* **2012**, *336*, 1011.
(25) Chandrasekhar, S. *Hydrodynamic and Hydromagnetic Stability*; Dover Publications: New York, 1981.
(26) Kassubek, F.; Stafford, C. A.; Grabert, H.; Goldstein, R. E. *Nonlinearity* **2001**, *14*, 167.
(27) Burki, J.; Goldstein, R. E.; Stafford, C. A. *Phys. Rev. Lett.* **2003**, 91.
(28) Burki, J.; Stafford, C. A. *Appl. Phys. a-Mater. Sci. Process.* **2005**, *81*, 1519.
(29) Burki, J.; Stafford, C. A.; Stein, D. L. *Phys. Rev. Lett.* **2005**, 95.
(30) Urban, D. F.; Buerki, J.; Stafford, C. A.; Grabert, H. *Phys. Rev. B* **2006**, 74.
(31) Karim, S.; Toimil-Molares, M. E.; Ensinger, W.; Balogh, A. G.; Cornelius, T. W.; Khan, E. U.; Neumann, R. *J. Phys. D: Appl. Phys.* **2007**, *40*, 3767.
(32) Zhang, Y.; Xu, J.; Xu, P.; Zhu, Y.; Chen, X.; Yu, W. *Nanotechnology* **2010**, *21*, 285501.
(33) Xia, Q.; Chen, X.; Zhao, K.; Liu, J. *Mater. Chem. Phys.* **2008**, *111*, 98.
(34) Li, D.; Kaner, R. B. *J. Am. Chem. Soc.* **2006**, *128*, 968.
(35) Young, J. K.; Lewinski, N. A.; Langsner, R. J.; Kennedy, L. C.; Satyanarayan, A.; Nammalvar, V.; Lin, A. Y.; Drezek, R. A. *Nanoscale Res. Lett.* **2011**, 6.
(36) Valenzuela, R.; Cecilia Fuentes, M.; Parra, C.; Baeza, J.; Duran, N.; Sharma, S. K.; Knobel, M.; Freer, J. *J. Alloys Compd.* **2009**, *488*, 227.